A Classical Molecular Dynamics Study into the Effect of Si/Al Ratio and Silanol Nest Defects on Water Diffusion in Zeolite HY

[a]A.J. Porter, [a]A.J. O'Malley[*]

[a]Centre for Sustainable and Circular Technologies, Department of Chemistry, University of Bath, UK, BA2 7AY

** a.o'malley@bath.ac.uk*

Abstract

The diffusion of water confined in zeolite HY has been studied using classical molecular dynamics at 300 K to probe the effects of water loading, Si/Al ratio and silanol nest defect presence on the behaviour of water confined in Brønsted acidic FAU zeolites. Water loading, ranging from 5 wt% to 33 wt%, is shown to have a significant effect on diffusivity showing an increase by a factor of ~7 over the loading range, towards a maximum diffusivity. Upon probing the effect of Si/Al ratio (in a range of Si/Al = 5 to fully siliceous) water diffusivity tends to decrease with the concentration of Brønsted acid sites which show strong interactions with the water molecules and thus hinder molecular mobility. The average residence time of water adsorbed to each Brønsted acid site also decreased with both water loading and Si/Al ratio. Water diffusivity shows the highest dependency on Si/Al ratio at 18 wt% loading, as a lack of total mobility in the systems at the lowest loadings is observed (due to significant populations of water molecules being immobilised via interaction with the framework and Brønsted acid sites) and less of a dependence is observed at the highest loadings due to the prevalence of sorbate-sorbate interactions. Notably, silanol nest presence (at a concentration of 1 per unit cell) had no significant effect on the diffusivity of water in HY at any water loading or Si/Al ratio. Reasons considered for this lack of influence include silanol geometry and flexibility at ambient temperature, and potentially a lower effective charge density of the defect site.

1. Introduction

The study of water diffusion within zeolites is of great interest across a broad variety of fields,[1] such as water decontamination[2] and water softening – the largest use of zeolites by weight[3]. Water is also an important side product of many zeolite-catalysed reactions within the petrochemical industry. Approximately thirty thousand metric tons of synthetic zeolites are consumed per year where FAU zeolites, used in fluid catalytic cracking, account for 95% of this.[4] In all instances, the behaviour of water can have a significant effect on either the catalytic properties[5] or adsorption/separation properties[6] of zeolites. Therefore, this behaviour must be fully understood to optimise these processes and materials.

A variety of factors may affect the dynamical behaviour of confined water such as zeolite topology, composition, defect presence and water loading. The presence of counterions, in particular, Brønsted acid sites (BASs) (whereby H^+ is the charge compensating cation for each aluminium substitution in the framework), are of great significance to catalytic applications. Several complications arise when tuning the acidity of a zeolite. Lower Si/Al ratios result in a higher acid site density - increasing the probability of confined species encountering an active site. However, this increased aluminium content also leads to a less thermally stable material and lowers the acidity of each individual site.[7] These sites will also have complex effects on the mobility of confined species throughout the zeolite pore system and other dynamical phenomena[8-10]. The strong H-bonding capability of each Brønsted site to adsorbed species, even on small molecules which should demonstrate high diffusivity, has been demonstrated by a range of modelling[11-16] and spectroscopic studies[17-19].

Concerning the formation of defects in Brønsted acidic zeolites, of particular interest are silanol nests[20, 21] whereby a T (Si, Al) atom vacancy is created, and the remaining unsaturated oxygens are protonated. These are formed during the dealumination process, which is routinely undertaken to improve thermal stability[22] and tune the catalytic properties of the zeolite by modifying the acidic character of the framework[23] either through the formation of extra-framework aluminium[24], or through the addition of silanol groups which may also contribute to the acidity changes [25]. Despite this pivotal role, relatively little is known about these species, their stability[26] and their interaction with adsorbed molecules.

A number of papers investigate the diffusivity of water via both simulations, such as molecular dynamics (MD) or Monte Carlo (MC), and experimental techniques such as quasielastic neutron scattering (QENS) and pulsed-field gradient NMR (PFG NMR), in different zeolites[27-30]. Early studies by Parravano et al[31] probed water diffusion in zeolite X and Y – variants of the FAU structure type with approximate compositions in the study of Si/Al ratios = 1 and 2 respectively. They observed the difference in the effect of Na and Ca counter ions on the self-diffusion coefficient of water via PFG

NMR. They observed insignificant differences between NaX, CaX and CaY and that the diffusivity of confined water was approximately half of that of bulk water, where the relatively small observed hindrance was attributed to the large pores of FAU. Humplik et al.[27] investigated the effect of the Si/Al ratio on water transport in MFI zeolites via combined sorption and high-pressure infiltration experiments. They observed that, although the adsorption capacity increased by a factor of ~7 as the composition was varied from a fully siliceous sample to Si/Al = 100, the diffusivity was lowered by up to 2 orders of magnitude. Ari et al.[28] carried out a comparable computational study, exploring the effect of sodium cations in MFI zeolites by variation of the Si/Al ratio across sample composition ranging from Si/Al = fully siliceous, 191 and 95. Diffusion coefficients were reduced by a factor of ~5 at 297 K at the lowest Si/Al ratio of 95 compared to the fully siliceous structure. Paoli et al.[29] applied QENS and PFG NMR to study the diffusion of water in NaCaA samples of varying calcium content. A negative correlation between the relative concentration of Ca ions and the diffusivity of water was observed.

Across all the studies a clear trend is observed that an increase in counterion concentration lowers the self-diffusivity of water. Although, it is important to note that Brønsted acid sites are significantly smaller than any other charge compensating cation which may be incorporated into the framework. This could cause considerable differences in their effect on diffusivity and adsorption. Studies pertaining to water adsorption in Brønsted acidic zeolites are present in the literature. Olson, Haag and Boghard[32] investigated the adsorption of water in H-ZSM-5 and found that the quantity of water adsorbed is proportional to the framework aluminium content. This higher adsorption is likely to lead to similar observations of other cations, mentioned above, that increasing the number of sites will reduce molecular diffusion. To our knowledge, no studies have investigated the influence of systematic variation of Brønsted acid site concentration on water diffusivity, in any zeolite topology.

There are also very few studies on the influence of silanol nests on water diffusivity in zeolites. Yazaydin and Thompson[30] utilized grand-canonical Monte Carlo (GCMC) alongside classical MD simulations to probe the effect of silanol nests and extra-framework cations on water structure, diffusion and adsorption within silicalite-1. Significant enhancement of the zeolite adsorption capacity was noted with the introduction of cations whilst silanol nests had a limited effect (lower by a factor of ~20) in comparison. Alkali metal addition also resulted in a decrease, by a factor of at least 10, in the self-diffusivity of water, similar to that shown in the previously mentioned MD study[28], with larger cations resulting in a greater decrease. However, silanol nest presence did not cause any significant change in diffusivity. Ahunbay[33] used MC simulations to probe water adsorption in MFI zeolites with sodium cations and silanol nests, finding that the increase in adsorption capacity caused by silanol nests was not significant.

Water loading is another factor which can have a significant effect on its diffusivity in the zeolite pores. Demontis et al[34] studied the diffusion of water at a range of loadings (approximately 2.7wt% to 34.6wt%) in NaX and NaY using both QENS and MD simulations. The self-diffusivity of water shows little change from 2.7wt% to 5.4wt%, grows at intermediate loadings from 5.4wt% to 16.6wt% and then plateaus at a maximum – above 16.6 wt% loading. Han et al[35] investigated the diffusion of water in VET and TON zeolites via MD simulations. They observed a decrease in unidirectional diffusivity, by approximately a factor of 4, when the loading was increased from 0.39 g/cm^3 to 2.1g/cm^3. It is clear from the literature that water diffusivity in zeolites also has a very complex relationship with sorbate loading, depending on a range of variables such as framework topology, pore size and composition. Krishna et al[36] composed a comprehensive review on this topic showing the large variety of dependencies observed, in the diffusion of many different molecules, in a range of zeolite topologies.

As mentioned, FAU type zeolites are one of the most widely applied in both catalysis and adsorption processes,[37] and can obtain a very wide range of Si/Al ratios through post-synthetic modification processes such as dealumination, which also lead to the introduction of defects such as silanol nests and extra-framework aluminium[21]. As previously noted, studies probing diffusion in FAU zeolites with Brønsted acid sites and silanol nests is very limited, especially with water as an adsorbate. We study the systematic variation on the number of Brønsted sites (Si/Al ratio) alongside the inclusion of silanol nests at a range of water loadings in zeolite HY. The effect of these factors on the self-diffusivity of water is reported herein.

2. Computational methods

We now discuss the construction, setup and running of our molecular dynamics simulations.

2.1 FAU framework

The 576 atom siliceous FAU cubic unit cell[38] (UC) with $Fd\bar{3}m$ symmetry was systematically substituted with aluminium to reach the Si/Al ratios of; fully-siliceous (0 Al per UC), 191 (1 Al per UC), 60 (3 AL per UC), 30 (6 Al per UC), 15 (12 Al per UC) and 5 (32 Al per UC). The aluminium atoms were placed as far apart as possible from their nearest neighbour to abide by Dempsey's rule[39] while accounting for the later implementation of periodic boundary conditions. The protons of the Brønsted acid sites (BASs) (denoted O_b-H_b) (figure 1A) were placed protruding into the supercage where possible. These unit cells formed the basis of the non-defective Brønsted acidic zeolite Y systems. To create the defective structures, one aluminium was removed from the unit cell, and the remaining unsaturated oxygens were protonated to create a silanol nest (denoted O_s-H_s) (figure 1B). These defective structures are herein referred to as the same Si/Al ratio as their defect-free counterparts for continuity. The silanol containing and defect-free unit cells were then extended to create 2 × 2 × 2 (48.5 Å × 48.5 Å × 48.5 Å) supercells of ca. 4600-4900 framework atoms – depending on Si/Al ratio and defect presence - and periodic boundary conditions were employed – figure 1. All visualisations of the zeolite systems are generated using Aten 2.1.9[40].

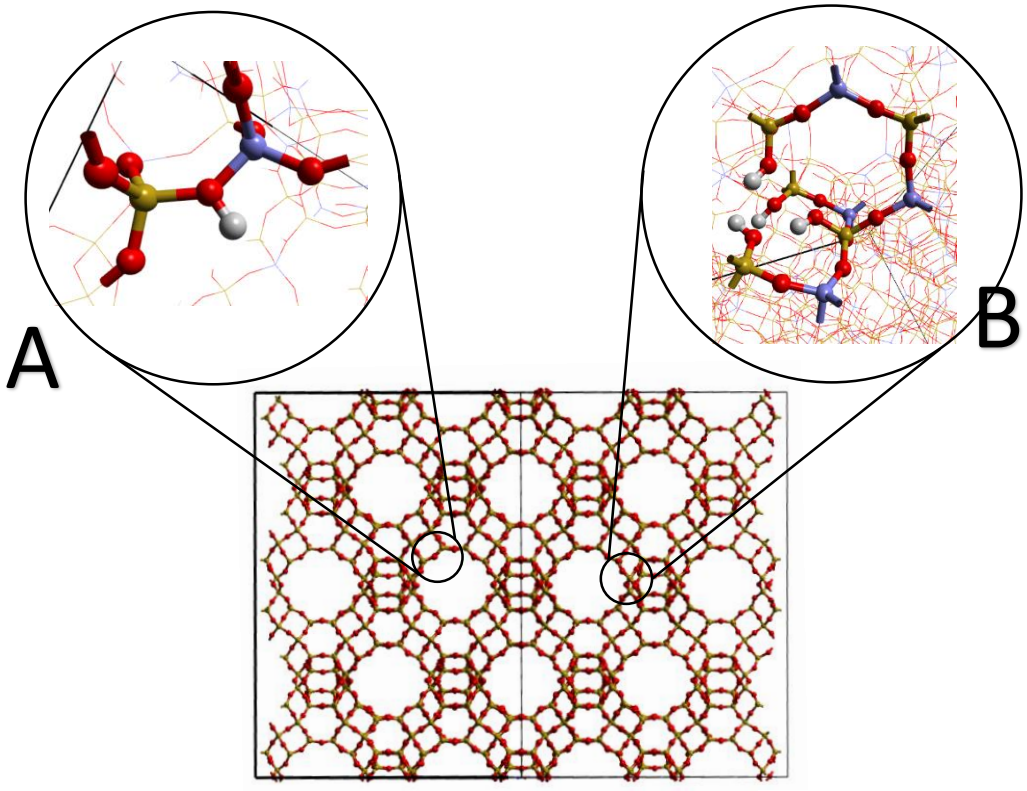

Figure 1. The siliceous zeolite HY supercell used, viewed from the 110 direction. Silicon (yellow), oxygen (red) and aluminium (blue). '**A**' shows a magnified snapshot of a Brønsted site in the Si/Al = 5 zeolite HY. '**B**' shows a magnified Snapshot of a silanol nest in the Si/Al = 5 zeolite HY.

A flexible model of the zeolite framework was used with the non-bonded interactions described using the potentials of Schröder et al[41], where the Si-O, Al-O and O-O interactions are represented by Buckingham potentials and the covalent O-H bonds of the Brønsted acid sites by a Morse potential. These potentials were developed mainly from empirical fitting to structural and physical properties of α-quartz, by Sanders et al[42], and Al_2O_3 and are assigned the framework atomic charges as in table 1. The three-body potential (used for mediating the O-Si-O and O-Al-O angles) was replaced by that of Ramsahye and Bell[43] which was found to maintain the stability of the flexible framework at low Si/Al ratios. These potentials are based on those from Kramer et al.[44] which are derived from ab initio methods and fitting to the vibrational spectrum of α-quartz. They have been slightly modified by scaling and further fitting to crystal data for MAP and Na-Y, both of which are zeolites with a high aluminium content similar to those in this work. We note that this aluminosilicate forcefield does not include a 4-body term for torsions in the framework. There is a potential here for a resulting difference in the framework flexibility, however this forcefield has previously facilitated the accurate calculation of the diffusivity trends of longer n-alkanes[45] in the comparatively smaller pore MFI structure – a system where the diffusivity would likely be more affected by any potential error introduced by neglecting this term due to the added steric hindrances. However, at the correct n-alkane, and also branched alkane loadings this forcefield has yielded values for the E_a of diffusion within experimental error of quasielastic neutron scattering measurements[46, 47]. We therefore consider the diffusivity in this far less sterically hindered system of water in FAU zeolites to be less affected by the lack of a torsional term in the framework forcefield, with the more significant components of the forcefield affecting the water mobility discussed later in this section. To describe the covalent O-H bonds of the silanol nest and the nonbonded interactions between the hydroxyl groups (which form the silanol nests and Brønsted acid sites), the potential model described by Du and de Leeuw[48] – who employed the zeolite model of Baram and Parker[49], based on Sanders fitting to α-quartz — were employed. This gave a Morse potential for the O_s-H_s covalent bond and Buckingham potentials for the non-bonded interactions between O_s-$O_{s/b}$ and O_s-H_s, where the subscript 's' denotes an atom relating to the silanol nest and the subscript 'b' to that of a Brønsted site. These potentials are derived from fitting to properties such as OH dissociation energy, stretching frequency and the interaction of OH with various cations described by Baram and Parker. A full list of the parameters used to model the framework is compiled in table 2.

Before water loading, the framework was equilibrated to 300 K via MD simulation using DLPOLY 4 code[50] in the NVT ensemble using a Berendsen[51] thermostat and a timestep of 0.5fs until thermal and energy fluctuations had stabilised, requiring at least 80 ps.

Charges	
Ion	**Charge**
Si	+4.000
Al	+3.000
O	-2.000
H_b	+0.426
H_s	+0.400
O_b	-1.426
O_s	-1.400

Table 1. Ionic charges of the zeolite framework used in the molecular dynamics simulations.

Zeolite-Zeolite interactions			
Buckingham Potential			
Atoms	**A (eV)**	**ρ (Å)**	**C (eV Å^6)**
Si-O	1283.907	0.32052	10.66158
Si-$O_{b/s}$	983.5566	0.32052	10.66158
O-O[a]	22764.0	0.149	27.88
O_s-$O_{s/b}$	22764.0	0.149	6.97
Al-O	1460.3	0.29912	0
Al-$O_{b/s}$	1142.6775	0.29912	0
O-H[b]	311.97	0.25	0
Morse Potential			
Atoms	**D (eV)**	**α (Å^{-1})**	**r_0 (Å)**
O_b-H_b	7.0525	2.1986	0.98450
O_s-H_s	7.0525	3.1749	0.92580
Three-body Potential			
Atoms	**k (eV rad^{-2})**		**θ (º)**
O-Si-O/$O_{b/s}$	12.1		109.47
O-Al-O/O_b	2.2		109.47

[a] O-O, O-O_b and O_b-O_b

[b] O-$H_{b/s}$, O_b-H_b and O_s-H_s

Table 2. Potential parameters of the zeolite framework used in the molecular dynamics simulations.

2.2 Water loading

Following the construction and equilibration of the empty framework supercells, water molecules were added as shown in figure 2. Mass fractions were calculated at 1.25 wt% (8 molecules per UC), 5 wt% (32 molecules per UC), 10 wt% (64 molecules per UC), 18 wt% (896 molecules per UC) and 33 wt% (1692 molecules per UC). The lowest loading, 1.25 wt%, was only used for testing in the siliceous cells as will be detailed later. The water molecules were described by a flexible TIP3P model derived by Schmitt and Voth[52], assigning the water oxygen (O_w) and hydrogen (H_w) charges of -0.834 and +0.417 respectively – the parameters of which are listed in table 3. The intramolecular bond stretching and bending parameters were derived to reproduce geometrical and energetic quantities of selected $H_3O^+ \cdot nH_2O$ clusters and refinement using quantum mechanical calculations. For the water-zeolite interactions, two sets of potentials have been used. Firstly, the potentials of Du and de Leeuw[48] (who also utilized the potential model of Sanders et al[42] for the zeolite framework) which were obtained from DFT calculations of water adsorption on α-quartz, are used to describe the interaction of water with the Brønsted sites, silanol groups and oxygen of the framework. Additionally, the potentials of Lewis et al[53] were used to describe the Si^{4+} and Al^{3+} interaction with water. These are an updated version of those from Du and de Leeuw which prevent the potentials from becoming critical at close range. Essentially, the repulsive term was increased to avoid very close contact of the water with these species which results in unfeasable structures. The full list of potentials is shown in table 2. We have used a relatively novel forcefield combination to describe this system using a mixture of Morse, Buckingham and Lennard-Jones potentials. To validate this, comparison between both theoretical and experimentally reported adsorption energies of water on both Brønsted acid sites and silanol nests was undertaken – to which good agreement was observed. More information can be found in section SI.1 of the supplementary information.

The water-containing cells were energy minimised to stabilise the initial configuration of water molecules loaded into the zeolite framework before the system was equilibrated.

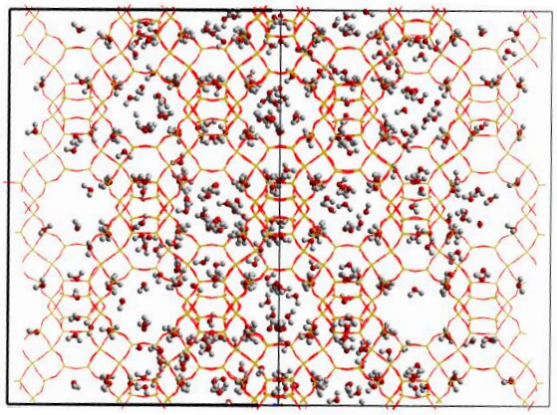

Figure 2. Snapshot of 10 wt% water loading in the siliceous FAU super cell.

Water interactions			
Buckingham Potential			
Atoms	**A (eV)**	**ρ (Å)**	**C (eV Å^6)**
Si-O_w	1283.907	0.32052	10.662
Al-O_w	1406.3	0.29912	0
O_w-O	22764.0	0.149	28.92
O_w-$O_{s/b}$	22764.0	0.149	17.14
O_w-$H_{w/s/b}$	396.27	0.25	10.0
H_w-$O_{s/b}$	311.97	0.25	0
H_w-O	396.27	0.25	0
Morse Potential[c]			
Atoms	**D (eV)**	**α (Å^{-1})**	**r_0 (Å)**
O_w-H_w	6.203713	2.22003	0.92376
Three-body Potential			
Atoms	**k (eV rad^{-2})**		**θ (°)**
H_w-O_w-H_w	4.1198		108.69
Lennard Jones Potential			
Atoms	**A (eV Å^{12})**		**B (eV Å^6)**
O_w-O_w	39344.98		42.15

[c] Specified as a bonding interaction between each pair.

Table 3. Potential parameters of the water-water and water-zeolite interactions.

2.4 Molecular dynamics runs and analysis

All MD simulations were run employing the DLPOLY 4 code[50] with a timestep of 0.5 fs, using a Van der Waals cutoff of 10 Å with the Coulombic interactions treated using the Ewald method. A Berendsen[51] thermostat was used to control the temperature in the canonical ensemble with all simulations set to 300 K. Each system was subject to the standardised format of completing an equilibration run in NVT, NVE and NVT ensemble, each for 80 ps to ensure the system reached minimal thermal and energetic fluctuations. The production run was then carried out for 2 ns in the NVE ensemble at 300 K, in a similar range to those referenced [27, 31] and the PFG-NMR in reference [29], allowing an additional 100 ps prior to this as the system stabilises in the new ensemble. The positions of the atoms were recorded once every picosecond resulting in 2000 records of the atomic positions. To quantify the diffusivity of the water molecules, the self-diffusion coefficient (D_s) was calculated. This involved tracking the positions of the oxygen atom of each water molecule and calculating the mean squared displacement (MSD) across all molecules for each step of the simulation. The Einstein relation was then used to calculate the D_s as shown in equation 1, provided the log(MSD)-log(t) relationship

$$D_s = \frac{1}{6}\lim_{t\to\infty}\frac{d}{dt}[\{r(t) - r(0)\}^2] \quad (1)$$

was linear.

The method of multiple time origins was used to improve the statistics of each simulation. An MSD plot of the first 1 ns of the production run was taken, with further MSDs taken starting at an offset of 1 ps from the origin (i.e. 0-1000 ps, 1-1001 ps, 2-1002 ps, etc) until the whole 2 ns simulation was covered. The average of the resulting 1000 × 1 ns MSD plots was then taken, from which the diffusion

coefficient was then calculated. The diffusion coefficient was calculated from the linear portion of the MSD plot, adhering to the Einstein relation. To remain consistent across all systems, this was taken from 200 ps to 1 ns of the MSD as all systems remain linear in this portion. The error was evaluated by calculating the variance of four diffusion coefficients, each calculated over 200 ps portions of the MSD used to calculate the diffusion coefficient.

To probe both the differing sorbate-sorbate interactions and the sorbate zeolite interactions in each MD run, radial distribution functions (RDFs) were calculated using the atom trajectories from the MD simulations. This was carried out using the integrated module for RDFs within the Visual Molecular Dynamics[54] package.

To probe the interactions between the water molecules and the Brønsted acid sites, specifically in terms of residence times, the contact correlation function between O_w and H_b was calculated as detailed in section SI.2 in the supplementary informaton.

3. Results and discussion

3.1 Effect of water loading on diffusivity

We now discuss the effect of water loading on self-diffusion in the defect-free siliceous and Brønsted acidic zeolite Y systems. The MSD plots for the defect-free siliceous and Brønsted acid containing Si/Al = 5 systems at 1.25 wt%, 5 wt%, 10 wt%, 18 wt% and 33 wt% water loadings are shown in figure 3 and their associated diffusion coefficients are listed in table 4. All MSD plots may be found in figure S2. The linear nature of the MSD plots, from 5 wt% loading and above, validates the use of the Einstein relation to calculate the diffusion coefficient. The lowest loading (1.25 wt%) does not show a linear increase with time (as shown in figure 3a) and therefore is not suitable for calculating self-diffusivity.

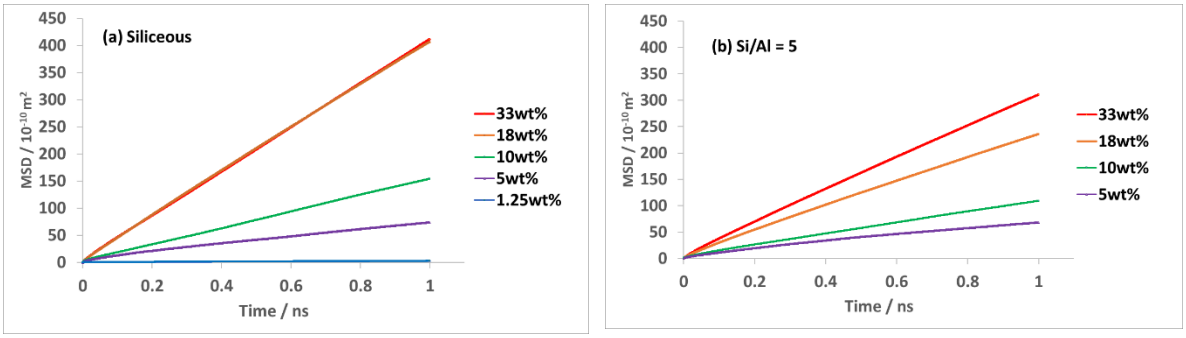

Figure 3. Mean squared displacement plots of 1.25 wt% (siliceous only), 5 wt%, 10 wt%, 18 wt% and 33wt% water loading in the fully siliceous and Si/Al = 5 zeolite Y systems.

Self-diffusion coefficients (10^{-10} m^2s^{-1})				
Loadings	**5wt%**		**10wt%**	
Si/Al Ratio	**Defect free**	**Silanol Containing**	**Defect Free**	**Silanol Containing**
Siliceous	1.088 ± 0.053	N/A	2.553 ± 0.089	N/A
191	1.368 ± 0.047	1.233 ± 0.052	2.368 ± 0.250	2.899 ± 0.200
60	1.254 ± 0.396	1.116 ± 0.228	2.229 ± 0.562	2.671 ± 0.122
30	1.039 ± 0.205	0.829 ± 0.074	2.264 ± 0.038	2.537 ± 0.253
15	1.100 ± 0.163	0.950 ± 0.023	2.045 ± 0.014	2.328 ± 0.196
10	0.832 ± 0.049	0.992 ± 0.011	2.215 ± 0.111	1.630 ± 0.052
5	0.995 ± 0.204	0.821 ± 0.132	1.737 ± 0.017	1.418 ± 0.048
Loadings	**18wt%**		**33wt%**	
Si/Al Ratio	**Defect free**	**Silanol Containing**	**Defect free**	**Silanol Containing**
Siliceous	6.647 ± 0.212	N/A	6.490 ± 0.100	N/A
191	6.288 ± 0.017	6.203 ± 0.078	6.328 ± 0.081	6.810 ± 0.302
60	6.168 ± 0.210	5.797 ± 0.054	6.794 ± 0.014	6.132 ± 0.017
30	6.000 ± 0.160	5.875 ± 0.087	6.279 ± 0.150	6.481 ± 0.382
15	4.969 ± 0.150	5.187 ± 0.179	5.832 ± 0.060	5.757 ± 0.149
10	4.597 ± 0.158	4.504 ± 1.127	5.443 ± 0.090	5.552 ± 0.002
5	3.768 ± 0.145	3.325 ± 0.144	5.009 ± 0.180	4.770 ± 0.011

Table 4. Diffusion coefficients in 10^{-10} m^2s^{-1}, and their errors, of water at 5 wt%, 10 wt%, 18 wt% and 33 wt% water loading in the fully siliceous and Si/Al = 191, 60, 30, 15, 10 and 5 zeolite Y systems.

At the very lowest loading (1.25 wt%), even in the siliceous framework where no adsorption sites are present, no water diffusion is observed over the timescale of our simulations. It was observed that the low number of water molecules in the system prevents the formation of intermolecular water-water hydrogen bonds, necessary to break the strong interactions of water with the zeolite framework. This strong interaction between the water hydrogens and framework oxygens of the siliceous Y system, illustrated in figure 4, is still present at a loading of 5 wt% – hindering diffusion – and further illustrated by the RDF in figure 5 which probes the interaction of water with the zeolite pore wall. Despite this system showing some diffusive behaviour, a clear coordinated structure is observed. Two peaks are shown at very close coordination of 2.75 Å and 3.55 Å indicating direct water-zeolite interactions. This is followed by a plateau and then a small peak at 5.35 Å indicating either a secondary coordination shell or a water molecule sited adjacent to that of the primary coordinated water. Beyond this, a drop is observed at ~6.5 Å which we consider is due to the smaller probability that a molecule lies within the centre of the zeolite supercage (diameter of 13 Å) – as opposed to residing at the pore surface where it can form more favourable bonds. The peaks at 2.75 Å and 3.55 Å relate to the coordination structure shown in figure 4 whereby the water is in an orientation where it can maximise the number of favourable interactions, forming 6 hydrogen bonds between the water hydrogens and zeolitic oxygens, as shown by the orange and blue lines – in figures 4A and B. Although the water looks to be in very close proximity to the oxygens of the framework, counter to intuition, the $O_w - O_{zeo}$ distance lies between 2.5 – 3 Å, matching that of bulk water. The RDF peak at 2.75 Å in figure 5 indicates the shortest $O_{zeo} - H_w$ bond to the two oxygens directly below the water molecule, and the peak at 3.55Å corresponds to the 4 more distant $O_{zeo} - H_w$ bonds. This latter peak shows the highest intensity of the whole plot indicating the highest occurrence of this interaction – due to there being a total of 4 interactions per water molecule – as opposed to the two relating to the shorter bond.

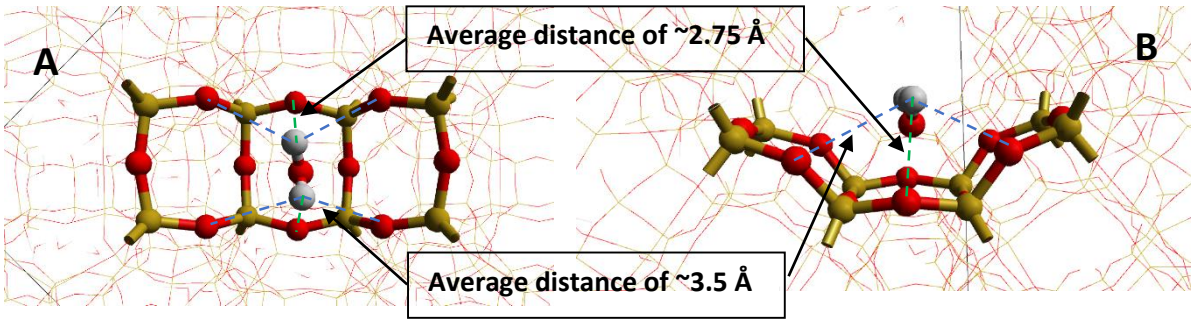

Figure 4. Snapshot of a water molecule bonding with the zeolite framework at 5 wt% loading in the purely siliceous system. (A) viewed from the 001 direction (B) viewed from the 110 direction. The blue and green lines indicate hydrogen bonding.

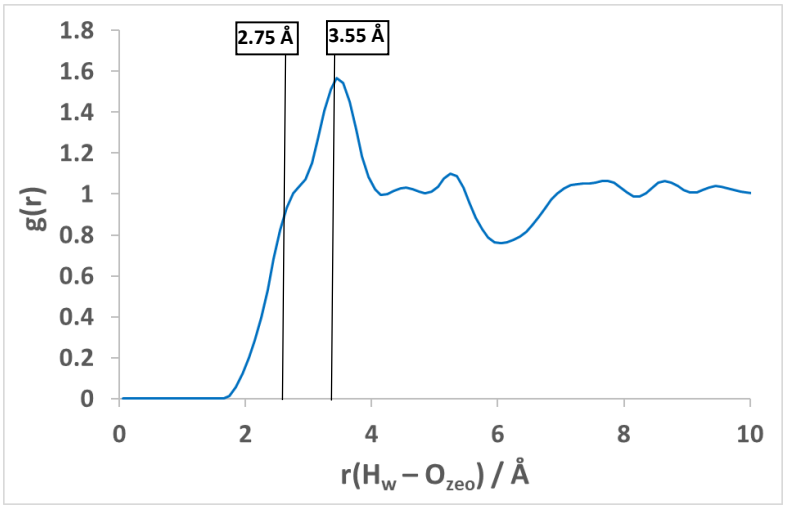

Figure 5. RDF between the water hydrogen (H_w) and zeolitic oxygen (O_{zeo}) at 5 wt% loading in the purely siliceous system.

In all systems, regardless of Si/Al ratio, an increase in diffusivity is observed between 5 and 18 wt% water loading – seen in figure 6. This is illustrative of the decreasing likelihood of water being able to directly interact with the pore wall, or adsorption sites for prolonged periods due to interactions with more freely diffusing water molecules – discussed later. Beyond 18 wt% loading, sorbate-sorbate interactions appear to be more significant in determining the rate of diffusion over the sorbate-zeolite interactions. In more siliceous systems, this may lead to a drop in diffusivity discussed later in terms of the RDF plots in figure 7. This trend with diffusivity was also observed by Demontis et al.[34] whereby an increase in water diffusivity was noted up to a similar loading, after which it did not increase significantly. The plateau between 18 and 33 wt% is not consistent in all systems, although the increase in diffusivity is less significant and may potentially reverse beyond this loading, due to steric hindrance and strong sorbate-sorbate interactions.

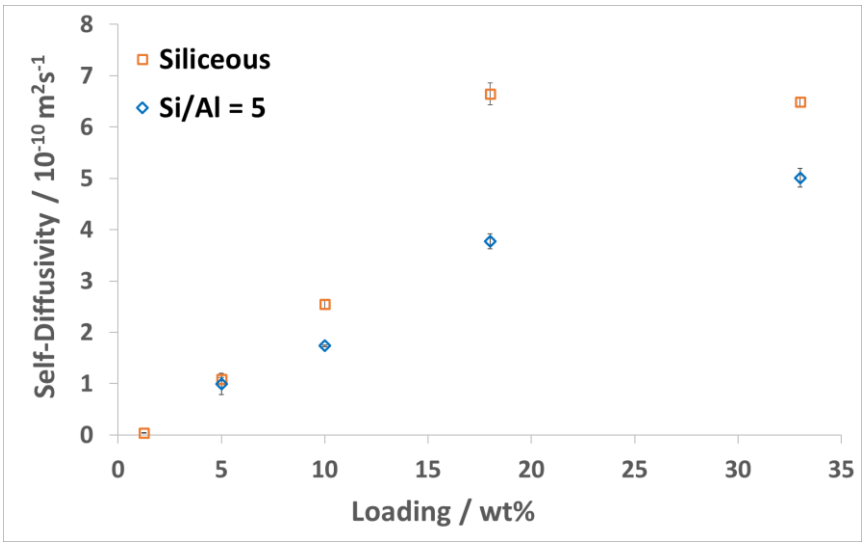

Figure 6. Diffusion coefficient of water at 1.25, 5, 10, 18 and 33 wt% loading in the purely siliceous (orange squares) and Si/Al = 5 (blue diamonds) zeolite Y systems.

We show in figure 6 the trend in diffusivity with loading for the siliceous system and the system with the highest concentration of Brønsted acid sites. A gradual increase in diffusivity is shown between 5 and 18 wt% after which a plateauing or decrease is observed, especially in the more siliceous systems. This trend in diffusivity with loading is largely observed throughout all zeolite compositions – shown in table 4. We note that a decrease in diffusivity between 18 and 33 wt% is observed in the more siliceous zeolite structures which we consider may be due to the lack of Brønsted sites, allowing a more significant increase in diffusivity at 18 wt% loading, before sorbate-sorbate interactions to play a more prominent role at the highest loading.

The difference in the range of diffusivity observed is shown in figure 6. As the Si/Al ratio is decreased the range of diffusivities also decreases from ~1.0 – 6.6×10^{-10} m^2s^{-1} in the siliceous system to ~1.0 – 5.4×10^{-10} m^2s^{-1} in the Si/Al = 5 system. Throughout all systems, we observe a general trend towards decreased diffusivity with aluminium content – a detailed discussion of diffusivity as a function of Si/Al ratio may be found in section 3.2.

To further probe the effect of loading at the upper extreme, a radial distribution function plot of the distance between water oxygens was calculated and is shown in figures 7a and b. These plots illustrate the water structure within the zeolite pores at 10 and 33 wt% loadings within the Si/Al = 5 and the siliceous system. In all cases, an initial peak at 2.75 Å – indicating the equilibrium distance between two water molecules – was present. At the 10 wt% loading, secondary and tertiary coordination peaks at 4.5, 6, 8 and 9 Å are observable in both zeolite systems – this suggests that ordered water clusters are forming with distinct coordination spheres throughout the zeolite Y supercage. At 33 wt%, however, the initial peak is far less intense – showing that a smaller proportion of the water molecules lie in direct contact with each other. Due to the much higher loading, single water molecules are further coordinated with a larger number of other waters and are thus encouraged to maximise the total number of interactions. The strongest (almost dimeric) water-water interactions are quickly broken by additional sorbate-sorbate interactions at high loading. The 3 – 6 Å region, therefore, becomes more populated and, due to the extreme crowding of water, the formation of ordered clusters is less likely. Additionally, it should be noted that the secondary structure is more pronounced in the siliceous framework than in the framework with Si/Al = 5. This illustrates how the Brønsted acid sites disrupt the coordination between the water molecules by preferentially forming sorbate-zeolite H-bonds and therefore disrupting the long-range order in the water structure.

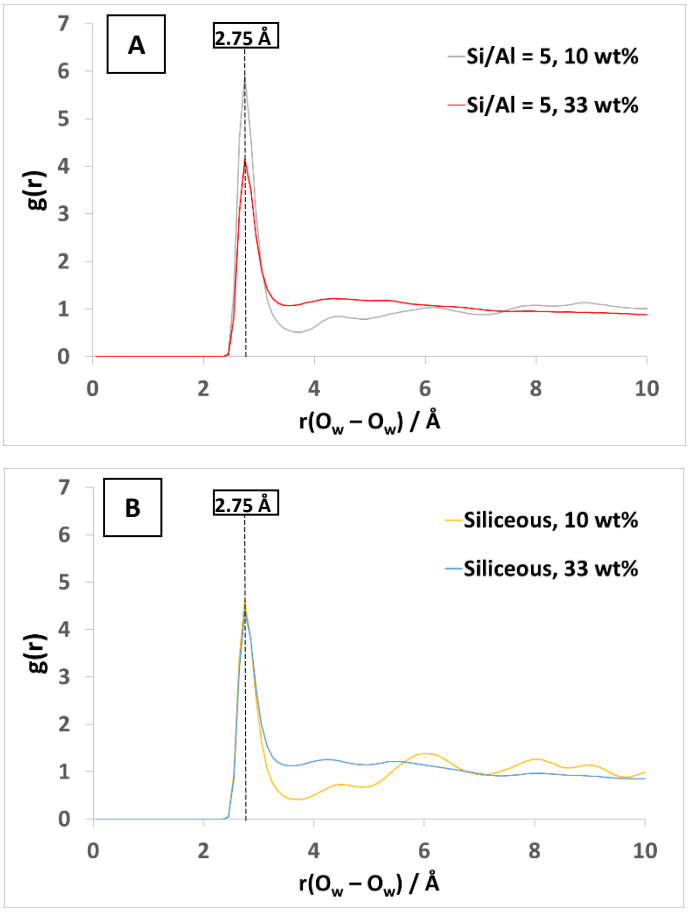

Figure 7. Radial distribution functions of water O_w – O_w at 10 wt% and 33 wt% loading in the siliceous and Si/Al = 5 systems.

We can therefore explain the observed trend in D_s with loading. At very low loadings water molecules are strongly bound to the framework via hydrogen bonding to Brønsted sites or the framework oxygen as shown in figure 4. As these sites reach saturation the remaining water molecules can no-longer bind to these sites and thus total diffusivity increases. Additionally, as more water is added, sorbate-sorbate interactions become more prominent and the likelihood of these interactions breaking the adsorption of surface-bound water increases, thus increasing the probability of movement and therefore overall diffusion. At a critical point above 18wt% loading, both favourable sorbate-sorbate interactions and steric hindrance of water diffusion under the confinement of the zeolite Y pores, leads to a plateauing and even a decrease in diffusivity to be observed as the crowding slows the overall motion of each water molecule. This is generally observed at all Si/Al ratios in zeolite HY. This is further examined by calculation of the coordination number of water which is seen to increase roughly 5 fold from <1 at 5 wt% to ~3.5 at 33 wt% as seen in supplementary information section SI.3.

3.2 Effect of Si/Al ratio on diffusivity

We now discuss the effect of Brønsted acid site density (Si/Al ratio) on water diffusivity. The MSD plots of water in zeolite HY at 10 and 18 wt% loadings as a function of Si/Al ratio are shown in figure S4. At 10 wt%, we see a general increase in diffusivity with Si/Al ratio. At 18 wt%, the same trend is observed. All plots, which may be viewed in figure S4 are indicative of diffusive behaviour from 5-33% loading.

The self-diffusion coefficients of water in zeolite Y as a function of Si/Al ratio are plotted in figure 9. The general increase in diffusivity from Si/Al = 5-30 is particularly clear at higher loadings as is reflected in the diffusion coefficient values listed in table 4. The decrease in diffusivity at high Brønsted acid site density is attributed to strong hydrogen bonding between water molecules and Brønsted acid sites of zeolites – shown to have adsorption energies of c.a. -72 to -84 kJmol^{-1} in previous DFT studies[55]. This adsorption and resultant coordination structure is further illustrated later.

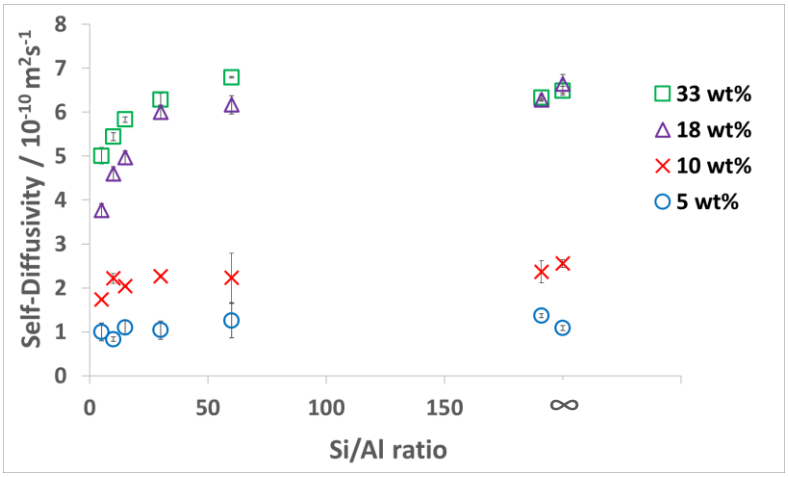

Figure 8. Diffusion coefficient of water at 5, 10, 18 and 33 wt% loading in the fully siliceous and Si/Al = 191, 60, 30, 15, 10 and 5 zeolite Y systems.

In figure 8 an 'r shaped' curve is observed, where the D_s is highly dependent on Si/Al ratio between Si/Al = 5 – 30, and a plateauing is observed approaching the higher ratios (lower acid site density). Notably, the dependence of water diffusivity, as an absolute value, on the Si/Al ratio is most stark at 18 wt% loading. At 5 wt% loading, the diffusivity ranges from ~1.0-1.4 × 10^{-10} m^{2}s^{-1} (40% increase) with Si/Al ratio although the upward trend in diffusivity with increasing Si/Al ratio is much less clear than that observed at higher loadings, especially when taking errors into account. At 10 wt% loading we see a general trend increasing from ~1.7 – 2.5 × 10^{-10} m^{2}s^{-1} (47% increase) followed by ~3.8 – 6.7× 10^{-10} m^{2}s^{-1} (76% increase) at 18 wt% loading (the largest difference as discussed) and ~5.0 – 6.5 × 10^{-10} m^{2}s^{-1} (30% increase) at 33 wt% loading.

An alternative approach to presenting the data is with diffusivity as a function of the number of Brønsted acid sites per water molecule as in figure 9. This reflects more clearly both the effects of loading and how increasing the aluminium content decreases the diffusivity. Again, the 5 and 10 wt% loading systems do not show a clear change in D_s with Brønsted acid sites per water, due to its small range in diffusivity. The two highest loadings, however, show clear negative correlations between D_s and Brønsted acid sites per water, in line with the very strong adsorption energy shown in the referenced DFT studies[55].

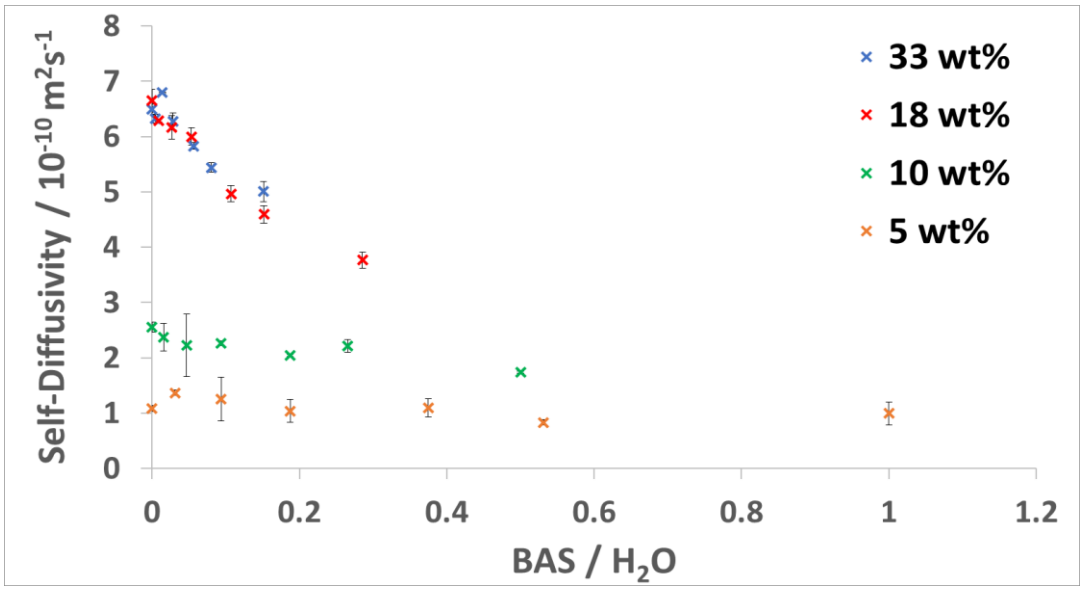

Figure 9. Diffusion coefficients of water at 5, 10, 18 and 33 wt% loading within the defect free systems as a function of the number of Brønsted acid sites per water.

The link between the effect of loading and Si/Al ratio on diffusivity is further probed using RDF plots between the Brønsted acid site hydrogen (H_b) and water oxygen (O_w) – in the Si/Al = 5 system at 5 wt% and 33 wt% loadings shown in figure 10. The main feature of this plot is the peak at ~2.5 Å indicating the hydrogen bonds between the Brønsted acid sites and water molecules. In the 5 wt% plot, this peak is far more intense than in the 33 wt% system, indicating a far higher proportion of the water molecules in this system are interacting strongly with a Brønsted acid site. At 33 wt% loading, the Brønsted acid sites are beyond their saturation point and sorbate-sorbate interactions have become more prominent. A clear shoulder at 3.5 Å is observed at 5 wt% water loading but not 33 wt%, at this low loading it is more likely the shoulder is due to secondary coordination, which is not possible at the highest loading as the large portion of non-coordinated water molecules further away from the pore surface at 33 wt% may inhibit secondary coordination due to strong sorbate-sorbate interactions.

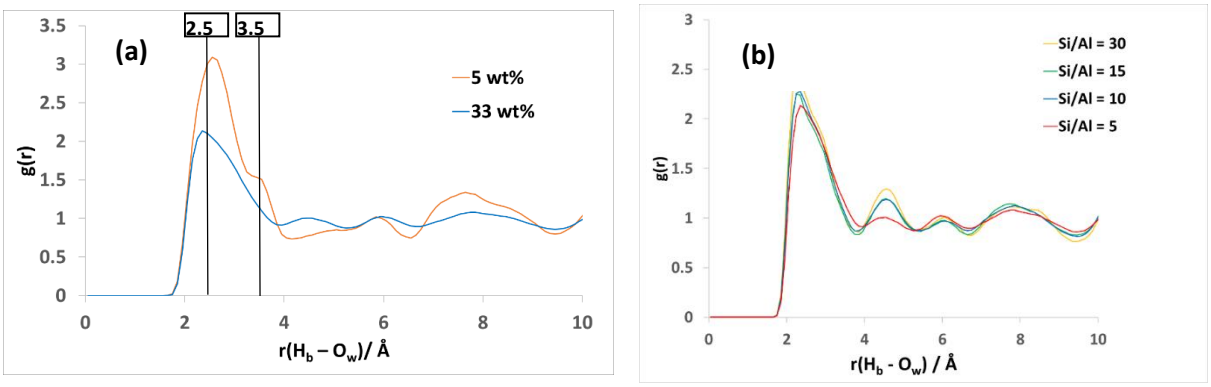

Figure 10. RDF plot of the Hb-Ow hydrogen bond in (a) the Si/Al = 5 zeolite Y system at 5 and 33 wt% and (b) at 33 wt% loading in the Si/Al = 5, 10, 15, and 30 zeolite Y systems.

To further investigate the relationship between the Brønsted acid site density and diffusivity at higher loadings, the Brønsted hydrogen (H_b) and water oxygen (O_w) RDF was calculated at 33 wt% across a range of Si/Al ratios shown in figure 10b.

The RDF for Si/Al = 191 and 60 are omitted due to the poor statistics of only 1 or 3 Brønsted acid sites per unit cell. There is distinct coordination with the Brønsted sites in every case. A fairly broad initial peak at ~2.4 Å is observed in all Si/Al ratio systems. A clear secondary structure, with peaks at 4.6, 6.0 and 8.0 Å, is also observed. Very subtle differences between each systems' secondary structure are observed, most important of these is that the Si/Al = 5 system shows a markedly lower intensity region at ~4.6 Å. This suggests that at the lowest Si/Al ratio the secondary coordination at one site is disrupted, even at the higher loadings where secondary coordination may be more facilitated – this is most likely because different sites lie within very close proximity, as seen in figure 11 and therefore water within the secondary coordination shell is more likely to become associated with an adjacent site.

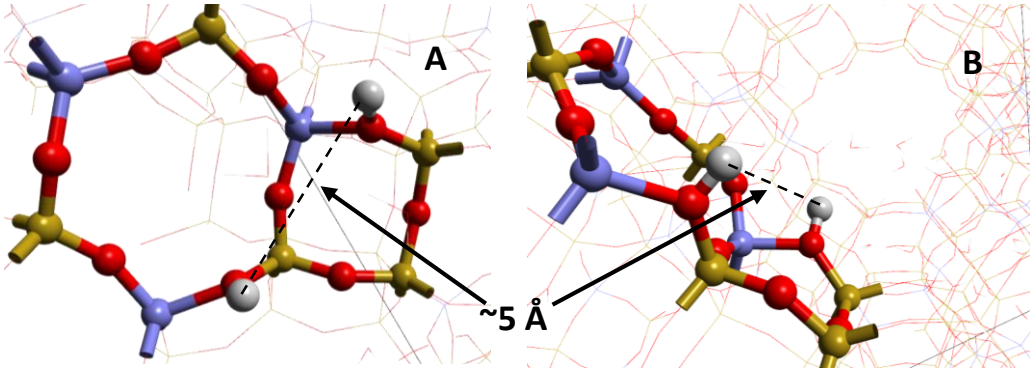

Figure 11. Proximate Brønsted acid sites in the Si/Al = 5 HY system.

Consistently we note that there appear to be two water bonding modes which both involve an interaction with the Brønsted acid sites itself and the zeolite framework. In both cases water H-bonds through both the Brønsted acid proton to water oxygen interaction (H_b-O_w) and water hydrogen (H_w) to framework oxygen (O_{zeo}) interaction. Some RDFs between various hydrogen bonding atoms of interest in the Si/Al = 15 system at 10 wt% loading are displayed below in figure 12a-c to show the modes of water-zeolite interactions which are present.

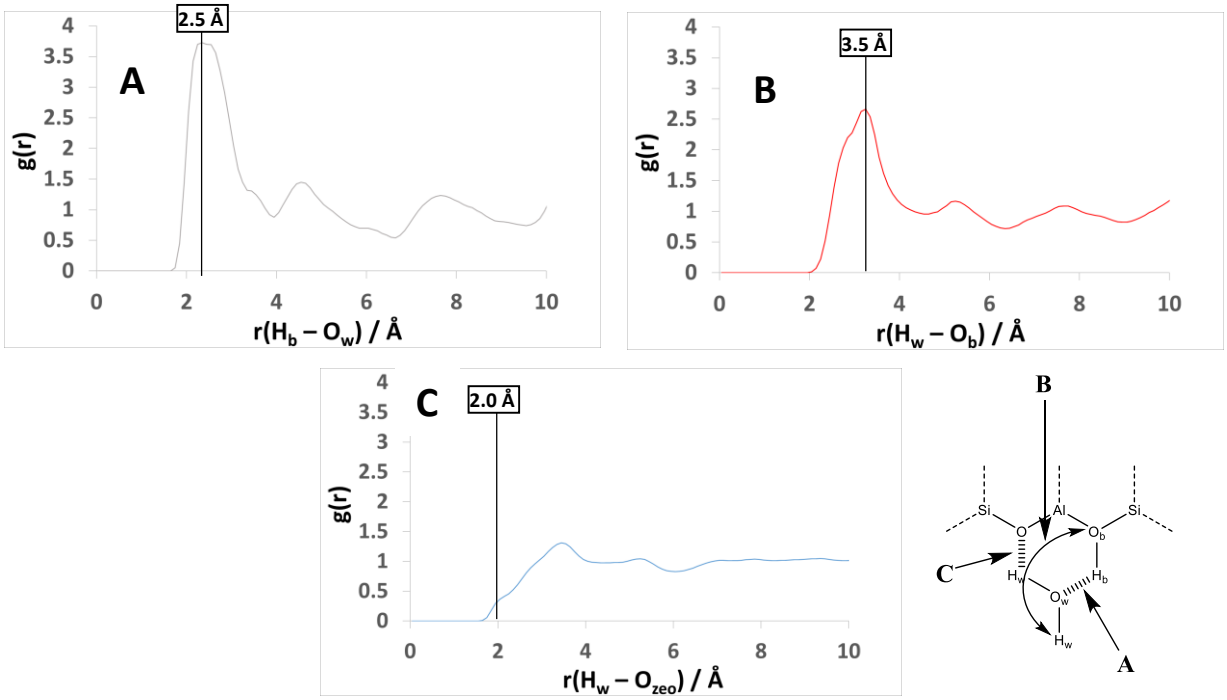

Figure 12. RDF between water and hydrogen bonding atoms at 10 wt% water loading within the Si/Al = 15 zeolite Y system. Figure A shows the H_b-O_w RDF, B the H_w-O_b RDF and C the H_w-O_{zeo} RDF. A schematic is included indicating the distances A, B and C.

Several features in the RDFs, figure 12, are of note and may be corroborated by the coordination depicted in figure 13. Firstly, we observe that there is clear water coordination with the Brønsted site, based on the intense initial peak, as shown in figures 12A and B. This bonding occurs at the shortest distance of 2.5 Å in the case of the H_b – O_w interaction, suggesting this is the strongest hydrogen bond, whereas the H_w – O_b interactions has a distance of 3.2 Å. Some coordination is also apparent between the water and the framework oxygen. We also observe a small shoulder at around 2 Å in the H_w – O_{zeo} RDF, figure 12C, which is most intense at the shortest distance of any RDF. This small shoulder suggests there is an additional strong interaction with the framework that does not occur as frequently. Together with the bonding observed upon visualisation of the water within the framework (figure 13), we can observe that this peak is caused by a two-fold interaction of the water between the framework oxygen and Brønsted site.

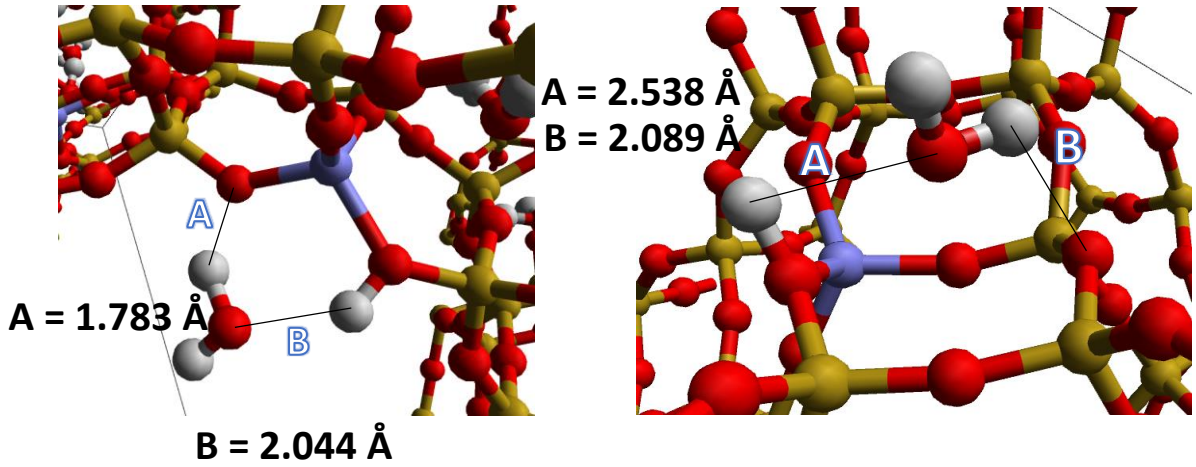

Figure 13. Two modes of water interacting with a Brønsted site.

To examine the adsorption of water to the Brønsted acid site further, an RDF plot between the water oxygens was produced as shown in figure 14. The first observed trend is that there is a negative correlation between Si/Al ratio and the probability that water molecules lie within their first (2.75 Å) or second coordination (4.45 Å) peak – shown by the decreasing size of the first peak as the Si/Al ratio increases. Contrasting this, as the amount of acid sites increase, water molecules are less likely to lie within the third (6.0 Å) and fourth (8.0 Å) coordination shell – which is likely sampling interactions between molecules at the pore surface and those in the supercage cavity. Due to the increased number of favourable interactions with the larger number of Brønsted sites. In summary, this means that the water molecules are clustering more tightly together when more Brønsted sites are present – in line with the strong coordination of multiple molecules to the acidic site. This trend mirrors that observed in the diffusivity whereby the lower the Si/Al ratio leads to stronger water clustering and, therefore, slower diffusion.

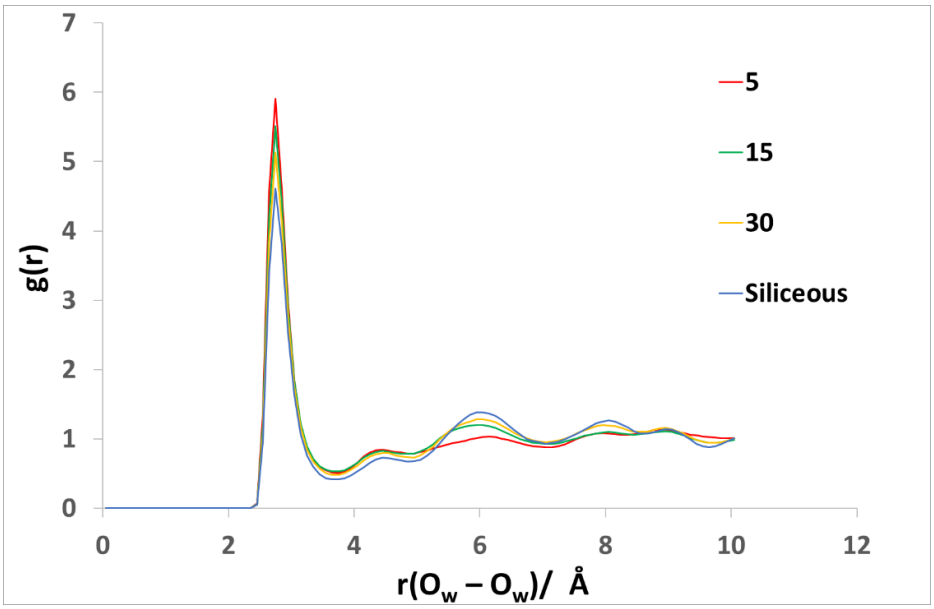

Figure 14. RDF between water oxygens at 10 wt% loading in the fully siliceous and Si/Al = 30,15 and 5 zeolite Y systems.

Contact correlation analysis between the water oxygen (O_w) and the Brønsted hydrogen (H_{zeo}) was also undertaken as described in section SI.2. This allowed for the determination of the average residence time of a water molecule adsorbed onto a Brønsted acid site further investigating the coordination between these species. Initially, the contact correlation function is calculated as per equation 2. A contact cut-off of 3.0 Å, as described in the methodology section, was used to investigate residence within the first coordination sphere. A single exponential function was then fit to this data, approximating that only one dynamical behaviour is taking place in this region – examples shown in figure S5. We note that while multiple behaviours would likely take place in the 3 Å region around the acid site (described by multiple exponentials which would give a better overall fit), the fitting of one exponential is sufficient to approximate an average comparison of residence times between systems and that the fitting to the lower time portion of the contact correlation plot is adequate. The residence time is quoted to one decimal place, although accuracy can only be assured to half a print step – i.e., 0.5 ps – as atomic coordinates were recorded once every picosecond. The residence time is then estimated for all the systems using similar plots. The resulting residence times are plotted in figure 15. The data point for the 5 wt% loaded Si/Al = 191 is omitted due to poor statistics.

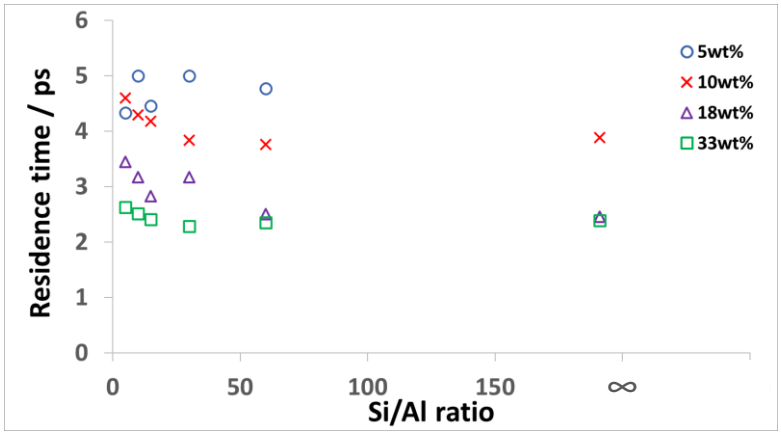

Figure 15. Residence times for water oxygens (O_w) to the Brønsted hydrogens (H_b)in zeolite HY at 5, 10, 18 and 33 wt% loading in the Si/Al = 191, 60, 30, 15, 10 and 5 zeolite Y systems.

A clear relationship between the loading and residence time is observed. Higher loadings resulted in a decreased residence time in direct contact with the acid site, with 33 wt% having an average residence time (t_r) of 2.4 ps, 18 wt% a t_r of 2.9 ps, 10 wt% a t_r of 4.0 ps and 5 wt% a t_r of 4.7 ps. This further demonstrates the increasing importance of the sorbate-sorbate interactions, as the loading increases, and the propensity of other water molecules to break the sorbate-zeolite interactions. Additionally, there appears to be an inverse correlation between the Si/Al ratio and the residence time – particularly in the case of the 33, 18 and 10 wt% systems – such that the more Brønsted acid sites present in the system the longer a molecule is likely to stay coordinated. We consider this is due to a lower quantity of 'free' water present and, as such, an adsorbed molecule is less likely to have its sorbate-zeolite interactions disrupted by interaction with a 'free' water molecule so on average the total mobility of water in the system is lowered as the Si/Al ratio is decreased.

3.3 Effect of silanol nest presence on water diffusivity

We now present the data pertaining to the silanol nest containing zeolite HY frameworks. The diffusivities as a function of loading and Si/Al ratio are plotted in figure S6. The relationship between diffusivity and both Si/Al ratio and loading is almost identical to the non-defective analogues. At 5 wt%, again, little correlation is observed with a range of D_s from ~0.8 – 1.2 × 10^{-10} m^2s^{-1} (50% increase); 10 wt% shows a clearer "r shaped" trend from ~1.4 – 2.9 × 10^{-10} m^2s^{-1} (107% increase); 18 wt% with diffusivities from ~3.3 – 6.2 × 10^{-10} m^2s^{-1} (88% increase), the widest range in absolute values, and finally at 33 wt% D_s of ~4.8 – 6.8 × 10^{-10} m^2s^{-1} (42% increase). We note that the highest Si/Al ratio dependency is, again, seen in the 18 wt% loaded system.

As the adsorbate-zeolite interaction between Brønsted sites and silanol nests (and the water molecules) are described by the Lennard-Jones potentials with a small difference in charges – see section 2.2 – a similar interaction and effect on diffusivity may be a logical expectation. Comparing figures 9 and S6, showing the D_s values for the defect-free and silanol containing systems, at all loadings the introduction of silanol nests has caused no significant difference in diffusivity. This is exemplified in figure 16a which compares the defect-free and silanol containing cells at the 18 wt% loading.

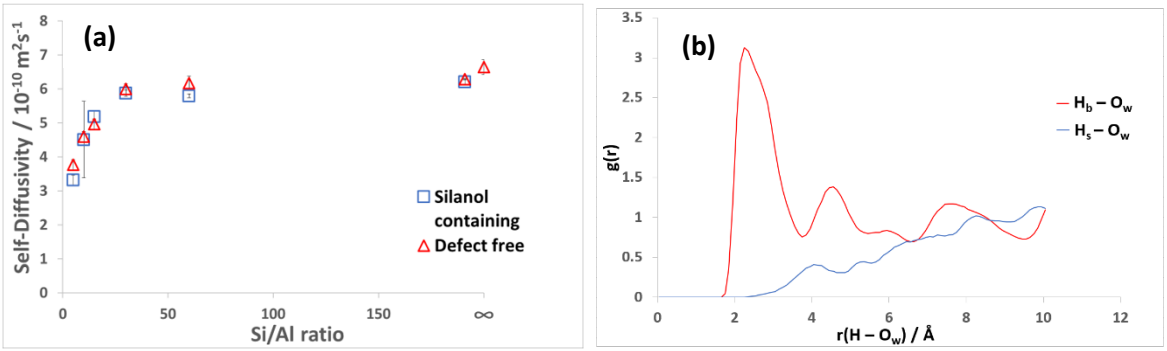

Figure 16. (a) Diffusion coefficient of water at 18 wt% loading within the silanol containing and defect free systems at different Si/Al ratios. (b) A comparison of the radial distribution functions of H_b (Brønsted) – O_w(water) and H_s (Silanol) – O_w(water) in the Si/Al = 15 system at 18 wt% water loading.

Comparing the diffusion coefficients in table 4, no consistent change in water diffusivity upon the introduction of silanol nests is observed, particularly when the errors in the D_s values are considered. These changes are likely due to alterations in the starting structure of the water at different loadings. Upon comparing the two systems directly an average decrease in diffusivity of 0.11 × 10^{-10} m^2s^{-1} is achieved at 5 wt% loading, an increase of 0.10 × 10^{-10} m^2s^{-1} at 10 wt%, an average decrease in diffusivity of 0.15 × 10^{-10} m^2s^{-1} at 18 wt% and decrease of 0.03 × 10^{-10} m^2s^{-1} at 33 wt% is observed on introduction of silanol nests. These changes are well within the errors of the D_s values, further displaying the limited effect silanol nests have on water diffusivity. We note that the number of silanol defects, at one per unit cell, within the structure is very low – compared to the number of Brønsted sites with a maximum of thirty-two per unit cell. This may mask any real effect which silanol nests may have. To further explore this one would need to create cells with higher defect density, though the extent to which this can be

done is fairly low as it will compromise the structural integrity of the framework. One possible explanation for the very small increase in diffusivity may simply be the removal of one Brønsted acid site to create the silanol nest defect.

An RDF plot of the silanol nest hydrogen (H_s) with the oxygen of water in comparison with the Bronsted acid site- water interaction is plotted in figure 16b. We observe that the coordination between silanol nest defects and water is very limited in comparison to the Brønsted acid systems. Upon comparing the H_b – O_w RDF and the H_s – O_w RDF in figure 16b this difference in coordination compared to the Brønsted sites is clear, as a very low population of water molecules are within 3 Å of each site. The closest proximity at which water is found to the silanol hydrogen H_s is also more distant, peaking at around 4 Å whereas in the case of the Brønsted site the first coordination shell is clear at 2 Å.

There are several possible reasons why the interactions between the silanol nest and the water molecules may be significantly less strong than the water interactions with Brønsted acid sites. We first consider the geometry of the silanol nest hydroxyls. The equilibrium geometry of the OH bonds typically results in the protons being vectored into the centre of the silanol nest defect, as seen in figure 17, causing them to be less accessible to a water molecule and therefore unable to regularly form long-lived hydrogen bonds. A clear contrast may be drawn between figures 1A and 17 whereby, the Brønsted site proton is protruding from the zeolite framework into the pore interior (figure 1A) unlike the silanol protons (figure 17). This grants the Brønsted acid proton a higher likelihood of coordination with water molecules as they diffuse past.

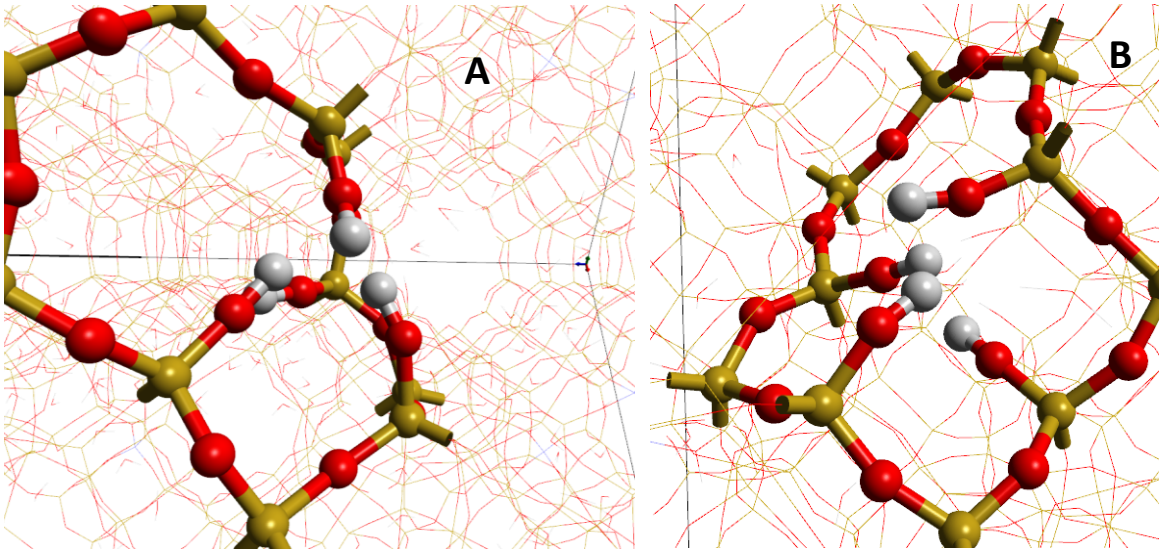

Figure 17. Visualizations of a silanol nest within the zeolite structure showing the vectoring of the silanol O-H bond.

Additionally, the silanol Si-O-H bond angle and torsions are more flexible than in a Brønsted site and are more prone to rotating and bending due to thermal motions, whereas the Brønsted acid sites are held more rigidly in position apart from the small O-H bond vibration and wagging motions of the O-H bond out of the Si-O-Al plane. These highly flexible motions result in the silanols competing and thus disrupting the water H-bonding with other silanols in the nest, as well as flexing away to regions not accessible for the water, such as inward into the framework structure.

We also note that the silanol nest defect has a lower effective charge density than a non-defective site. Specifically, the four silanol protons (a total charge of +1.704) have a significantly lower effective charge than the silicon or aluminium of the framework (a charge of +4/+3) which would be in the same location. This could lead to weaker electrostatic interactions between the defect and water in contrast to a framework Si or Al, resulting in a smaller likelihood of longer-term interactions with the silanol nest. Combined, these factors may well be responsible for the overall less significant interaction, and this general absence of diffusion hindrance between the water and the silanol nest.

4. Summary and conclusions

Classical molecular dynamics simulations were used to investigate the effect of loading, Si/Al ratio (and thus Brønsted acid site density) and silanol nest presence on the diffusion of water in zeolite HY. It was observed that increasing the water loading results in an increase in diffusivity by a factor of ~7 from 5 wt% up to 18 wt% loading in the siliceous Y system, and by a factor of ~ 4 in HY with Si/Al = 5. The diffusivity at the highest loading (33 wt%) was 6.6×10^{-10} m^2s^{-1} in the siliceous system and 5.0×10^{-10} m^2s^{-1} in the Si/Al = 5 system. Generally, the increase in diffusivity from 18 to 33 wt% loading is less stark and in fact, a slight decrease is observed in the two most siliceous systems (attributed to steric hindrance and strong sorbate-sorbate interactions). As the loading is increased, the residence time of a water molecule at each Brønsted site also decreases due to disruption of H-bonding between water and the acid sites from sorbate-sorbate interactions.

The Si/Al ratio and thus the concentration of Brønsted acid sites has a significant effect on water diffusivity. At 18 wt% water loading, a decrease of a factor of ~2 in D_s was observed upon increasing the aluminium content from a siliceous system to Si/Al = 5. Water loadings of around 18 wt% appear to be the critical loading region at which the effect of the Si/Al ratio is most pronounced. The effect of Si/Al ratio on diffusivity is far less clear at low loadings due to the significantly smaller proportion of non-framework coordinated water molecules and thus decreased chance of observing mobile water generally. The residence time of bound water molecules at acidic sites also increases with the number of Brønsted acid sites. At 18 wt% loading, we find that the residence time of water at each Brønsted site increases from 2.5 ps to 3.5 ps as we move from Si/Al = 191 to 5. Again, this loading exhibits the strongest dependence of residence time on Si/Al ratio.

The inclusion of silanol nests results in no consistent change in water diffusivity. This is corroborated by the observation of far less significant coordination between water and the silanol nest hydroxyls compared to Brønsted acid sites, as shown by plots of the radial distribution function. The far less significant interactions appear to be caused, mostly, by the geometry/orientation of the silanol nest hydroxyls, resulting in steric hindrance for water molecules accessing the site. Indeed, across all zeolite Y Si/Al ratios and water loadings, the average difference in diffusivity between the silanol nest containing systems and the defect-free systems is less than 0.2×10^{-10} m^2s^{-1}, with errors typically overlapping between defective and non-defective systems.

Acknowledgements

This work was supported by the UK Engineering and Physical Sciences Research Council (EPSRC) grant EP/R513155/1 for the University of Bath. This research made use of the Balena High Performance Computing (HPC) Service at the University of Bath. AJOM acknowledges Roger and Sue Whorrod for the funding of a Whorrod Fellowship. We would also like to thank Professor Steve Parker, Dr Carlos Hernandez Tamargo and Sandra McHugh for their valuable discussion and insight.

Associated Content

The supporting information document includes details on the forcefield validation, the method of calculating the contact correlation function and a description of how the size of water clusters were determined. Figures are also included associated with cluster size calculations, mean squared displacement plots, contact correlation fitting and plots of diffusion coefficients as a function of Si/Al ratio in the silanol containing HY systems.

References

1. Kärger, J.; Vasenkov, S.; Auerbach, S. M., Diffusion in zeolites. In *Handbook of Zeolite Science and Technology*, CRC Press: 2003; pp 458-560.
2. Margeta, K.; Logar, N. Z.; Šiljeg, M.; Farkaš, A., Natural zeolites in water treatment–how effective is their use. *Water treatment* **2013,** *5*, 81-112.
3. Cejka, J.; van Bekkum, H.; Corma, A.; Schueth, F., *Introduction to Zeolite Molecular Sieves*. 3 ed.; Elsevier Science: 2007; Vol. 168.
4. Millini, R.; Zou, X.; Strohmaier, K.; Schwieger, W.; Eliasova, P.; Morris, R. E.; Weckhuysen, B.; Zhou, W.; Abdo, S.; Martinez, A., *Zeolites in catalysis: properties and applications*. Royal Society of Chemistry: 2017.
5. Chen, K.; Damron, J.; Pearson, C.; Resasco, D.; Zhang, L.; White, J. L., Zeolite Catalysis: Water Can Dramatically Increase or Suppress Alkane C–H Bond Activation. *ACS Catalysis* **2014,** *4* (9), 3039-3044.
6. Krishna, R.; van Baten, J. M., Hydrogen Bonding Effects in Adsorption of Water−Alcohol Mixtures in Zeolites and the Consequences for the Characteristics of the Maxwell−Stefan Diffusivities. *Langmuir* **2010,** *26* (13), 10854-10867.
7. Derouane, E. G.; Védrine, J. C.; Pinto, R. R.; Borges, P. M.; Costa, L.; Lemos, M. A. N. D. A.; Lemos, F.; Ribeiro, F. R., The Acidity of Zeolites: Concepts, Measurements and Relation to Catalysis: A Review on Experimental and Theoretical Methods for the Study of Zeolite Acidity. *Catalysis Reviews* **2013,** *55* (4), 454-515.
8. Kärger, J., Measurement of Diffusion in Zeolites—A Never Ending Challenge? *Adsorption* **2003,** *9* (1), 29-35.
9. O'Malley, A. J.; Catlow, C. R. A., Chapter 6 - Sorbate Dynamics in Zeolite Catalysts. In *Experimental Methods in the Physical Sciences*, Fernandez-Alonso, F.; Price, D. L., Eds. Academic Press: 2017; Vol. 49, pp 349-401.
10. Jobic, H.; Theodorou, D. N., Quasi-elastic neutron scattering and molecular dynamics simulation as complementary techniques for studying diffusion in zeolites. *Microporous and Mesoporous Materials* **2007,** *102* (1), 21-50.
11. Pelmenschikov, A.; Van Santen, R., Water adsorption on zeolites: ab-initio interpretation of IR data. *The Journal of Physical Chemistry* **1993,** *97* (41), 10678-10680.
12. Greatbanks, S. P.; Hillier, I. H.; Burton, N. A.; Sherwood, P., Adsorption of water and methanol on zeolite Bro/nsted acid sites: An ab initio, embedded cluster study including electron correlation. *The Journal of chemical physics* **1996,** *105* (9), 3770-3776.
13. Haase, F.; Sauer, J., Ab initio molecular dynamics simulation of methanol interacting with acidic zeolites of different framework structure. *Microporous and Mesoporous Materials* **2000,** *35*, 379-385.
14. Nastase, S. A. F.; O'Malley, A. J.; Catlow, C. R. A.; Logsdail, A. J., Computational QM/MM investigation of the adsorption of MTH active species in H-Y and H-ZSM-5. *Physical Chemistry Chemical Physics* **2019,** *21* (5), 2639-2650.
15. O'Malley, A. J.; Logsdail, A. J.; Sokol, A. A.; Catlow, C. R. A., Modelling metal centres, acid sites and reaction mechanisms in microporous catalysts. *Faraday Discussions* **2016,** *188* (0), 235-255.
16. O'Malley, A. J.; García Sakai, V.; Silverwood, I. P.; Dimitratos, N.; Parker, S. F.; Catlow, C. R. A., Methanol diffusion in zeolite HY: a combined quasielastic neutron scattering and molecular dynamics simulation study. *Physical Chemistry Chemical Physics* **2016,** *18* (26), 17294-17302.
17. Parker, L.; Bibby, D.; Burns, G., Interaction of water with the zeolite HY, studied by FT ir. *Zeolites* **1991,** *11* (3), 293-297.
18. Anderson, M. W.; Klinowski, J.; Barrie, P. J., Proton magic-angle-spinning NMR studies of the adsorption of alcohols on molecular sieve catalysts. *The Journal of Physical Chemistry* **1991,** *95* (1), 235-239.

19. Omojola, T.; Silverwood, I. P.; O'Malley, A. J., Molecular behaviour of methanol and dimethyl ether in H-ZSM-5 catalysts as a function of Si/Al ratio: a quasielastic neutron scattering study. *Catalysis Science & Technology* **2020,** *10* (13), 4305-4320.
20. Garcia-Basabe, Y.; Rodriguez-Iznaga, I.; de Menorval, L.-C.; Llewellyn, P.; Maurin, G.; Lewis, D. W.; Binions, R.; Autie, M.; Ruiz-Salvador, A. R., Step-wise dealumination of natural clinoptilolite: Structural and physicochemical characterization. *Microporous and Mesoporous Materials* **2010,** *135* (1-3), 187-196.
21. Yan, Z. M.; Ding, M. A.; Zhuang, J. Q.; Liu, X. C.; Liu, X. M.; Han, X. W.; Bao, X. H.; Chang, F. X.; Xu, L.; Liu, Z. M., On the acid-dealumination of USY zeolite: a solid state NMR investigation. *Journal of Molecular Catalysis a-Chemical* **2003,** *194* (1-2), 153-167.
22. Beyer, H. K., Dealumination Techniques for Zeolites. In *Post-Synthesis Modification I*, Springer Berlin Heidelberg: Berlin, Heidelberg, 2002; pp 203-255.
23. Kühl, G. H., Modification of zeolites. In *Catalysis and Zeolites*, Springer: 1999; pp 81-197.
24. Wang, Q.; Giannetto, G.; Guisnet, M., Dealumination of zeolites III. Effect of extra-framework aluminum species on the activity, selectivity, and stability of Y zeolites in n-heptane cracking. *Journal of Catalysis* **1991,** *130* (2), 471-482.
25. Hoffmann, P.; Lobo, J. A., Identification of diverse silanols on protonated ZSM-5 zeolites by means of FTIR spectroscopy. *Microporous and Mesoporous Materials* **2007,** *106* (1-3), 122-128.
26. Senderov, E.; Halasz, I.; Olson, D. H., On existence of hydroxyl nests in acid dealuminated zeolite Y. *Microporous and Mesoporous Materials* **2014,** *186* (C), 94-100.
27. Humplik, T.; Raj, R.; Maroo, S. C.; Laoui, T.; Wang, E. N., Effect of Hydrophilic Defects on Water Transport in MFI Zeolites. *Langmuir* **2014,** *30* (22), 6446-6453.
28. Ari, M. U.; Ahunbay, M. G.; Yurtsever, M.; Erdem-Senatalar, A., Molecular dynamics simulation of water diffusion in MFI-type zeolites. *The journal of physical chemistry. B* **2009,** *113* (23), 8073.
29. Paoli, H.; Méthivier, A.; Jobic, H.; Krause, C.; Pfeifer, H.; Stallmach, F.; Kärger, J., Comparative QENS and PFG NMR diffusion studies of water in zeolite NaCaA. *Microporous and mesoporous materials* **2002,** *55* (2), 147-158.
30. Özgür Yazaydın, A.; Thompson, R. W., Molecular simulation of water adsorption in silicalite: Effect of silanol groups and different cations. *Microporous and Mesoporous Materials* **2009,** *123* (1), 169-176.
31. Parravano, C.; Baldeschwieler, J. D.; Boudart, M., Diffusion of Water in Zeolites. *Science* **1967,** *155* (3769), 1535-1536.
32. Olson, D.; Haag, W.; Borghard, W., Use of water as a probe of zeolitic properties: interaction of water with HZSM-5. *Microporous and Mesoporous Materials* **2000,** *35*, 435-446.
33. Ahunbay, M. G., Monte Carlo Simulation of Water Adsorption in Hydrophobic MFI Zeolites with Hydrophilic Sites. *Langmuir* **2011,** *27* (8), 4986-4993.
34. Demontis, P.; Jobic, H.; Gonzalez, M. A.; Suffritti, G. B., Diffusion of Water in Zeolites NaX and NaY Studied by Quasi-Elastic Neutron Scattering and Computer Simulation. *J. Phys. Chem. C* **2009,** *113* (28), 12373-12379.
35. Han, K. N.; Bernardi, S.; Wang, L.; Searles, D. J., Water diffusion in zeolite membranes: molecular dynamics studies on effects of water loading and thermostat. *Journal of Membrane Science* **2015,** *495*, 322-333.
36. Krishna, R.; Paschek, D.; Baur, R., Modeling the occupancy dependence of diffusivities in zeolites. *Microporous and mesoporous materials* **2004,** *76* (1-3), 233-246.
37. Abdo, S. F.; Wilson, S. T., Chapter 9 Zeolites in Industrial Catalysis. In *Zeolites in Catalysis: Properties and Applications*, The Royal Society of Chemistry: 2017; pp 310-350.
38. Meier, W. M.; Olson, D. H.; Baerlocher, C., Atlas of zeolite structure types. *Zeolites* **1996,** *17* (1-2), 1-229.
39. Dempsey, E., Aluminum ion distributions in zeolites. *Journal of Catalysis* **1977,** *49* (1), 115-119.

40. Youngs, T. G. A., Aten—An application for the creation, editing, and visualization of coordinates for glasses, liquids, crystals, and molecules. *Journal of Computational Chemistry* **2010,** *31* (3), 639-648.
41. Schröder, K.-P.; Sauer, J.; Leslie, M.; Richard, C.; Catlow, A.; Thomas, J. M., Bridging hydrodyl groups in zeolitic catalysts: a computer simulation of their structure, vibrational properties and acidity in protonated faujasites (H · Y zeolites). *Chemical Physics Letters* **1992,** *188* (3), 320-325.
42. Sanders, M. J.; Leslie, M.; Catlow, C. R. A., Interatomic potentials for SiO2. *Journal of the Chemical Society, Chemical Communications* **1984,** (19), 1271-1273.
43. Ramsahye, N. A.; Bell, R. G., Cation mobility and the sorption of chloroform in zeolite NaY: Molecular dynamics study. *Journal of Physical Chemistry B* **2005,** *109* (10), 4738-4747.
44. Kramer; Farragher; van Beest, B.; van Santen, R., Interatomic force fields for silicas, aluminophosphates, and zeolites: Derivation based on ab initio calculations. *Physical review. B, Condensed matter* **1991,** *43* (6), 5068.
45. O'Malley, A. J.; Catlow, C. R. A., Molecular dynamics simulations of longer n-alkanes in silicalite: a comparison of framework and hydrocarbon models. *Physical Chemistry Chemical Physics* **2013,** *15* (43), 19024-19030.
46. O'Malley, A. J.; Catlow, C. R. A., Molecular dynamics simulations of longer n-alkanes in silicalite: state-of-the-art models achieving close agreement with experiment. *Physical Chemistry Chemical Physics* **2015,** *17* (3), 1943-1948.
47. O'Malley, A. J.; Catlow, C. R. A.; Monkenbusch, M.; Jobic, H., Diffusion of Isobutane in Silicalite: A Neutron Spin–Echo and Molecular Dynamics Simulation Study. *The Journal of Physical Chemistry C* **2015,** *119* (48), 26999-27006.
48. Du, Z.; de Leeuw, N. H., A combined density functional theory and interatomic potential-based simulation study of the hydration of nano-particulate silicate surfaces. *Surface Science* **2004,** *554* (2), 193-210.
49. Baram, P.; Parker, S., Atomistic simulation of hydroxide ions in inorganic solids. *Philosophical Magazine B* **1996,** *73* (1), 49-58.
50. Todorov, I. T.; Smith, W.; Trachenko, K.; Dove, M. T., DL_POLY_3: new dimensions in molecular dynamics simulations via massive parallelism. *Journal of Materials Chemistry* **2006,** *16* (20), 1911-1918.
51. Berendsen, H. J. C.; Postma, J. P. M.; van Gunsteren, W. F.; Dinola, A.; Haak, J. R., Molecular dynamics with coupling to an external bath. *The Journal of Chemical Physics* **1984,** *81* (8), 3684-3690.
52. Schmitt, U. W.; Voth, G. A., The computer simulation of proton transport in water. *The Journal of Chemical Physics* **1999,** *111* (20), 9361-9381.
53. Lewis, D. W.; Ruiz-Salvador, A. R.; Almora-Barrios, N.; Gómez, A.; Mistry, M., Modelling of hydrated Ca-rich zeolites. *Molecular Simulation* **2002,** *28* (6-7), 649-661.
54. Humphrey, W.; Dalke, A.; Schulten, K., VMD: visual molecular dynamics. *Journal of molecular graphics* **1996,** *14* (1), 33-38.
55. Krossner, M.; Sauer, J., Interaction of water with Brønsted acidic sites of zeolite catalysts. Ab initio study of 1: 1 and 2: 1 surface complexes. *The Journal of Physical Chemistry* **1996,** *100* (15), 6199-6211.

For Table of Contents only